The Astrophysical Journal, 659:1761–1776, 2007 April 20

TRAPPING AND DIFFUSIVE ESCAPE OF FIELD LINES IN TWO-COMPONENT MAGNETIC TURBULENCE

P. Chuychai,[1] D. Ruffolo,[2] W. H. Matthaeus,[1] and J. Meechai[3]

Received 2006 August 28; accepted 2006 November 13

ABSTRACT

Recent studies have shown that transport along magnetic field lines in turbulent plasmas admits a surprising degree of persistent trapping due to small-scale topological structures. This underlies the partial filamentation of magnetic connection from small regions of the solar corona to Earth orbit, as indicated by the observed dropouts (i.e., inhomogeneity and sharp gradients) of solar energetic particles. We explain the persistence of such topological trapping using a two-component model of magnetic turbulence with slab and two-dimensional (2D) fluctuations, which has provided a useful description of transport phenomena in the solar wind. In the presence of slab turbulence, the diffusive escape of field lines from 2D orbits is suppressed by either a strong or an irregular 2D field. For slab turbulence superposed on a 2D field with a single, circular island, we present an analytic theory, confirmed by numerical simulations, for the trapping length and its dependence on various parameters. For a turbulent 2D+slab field, we find that the filamentation of magnetic connectivity to the source is sharply delineated by local trapping boundaries, defined by a local maximum in the mean squared field along the 2D orbit, because of a similar suppression effect. We provide a quasi-linear theory for field-line diffusion in a turbulent 2D+slab field, which indicates that irregularity of the 2D orbit enhances the suppression of slab diffusion. The theory is confirmed by computer simulations. These concepts provide a physical explanation of the persistence and sharpness of dropouts of solar energetic particles at Earth orbit.

Subject headings: diffusion — interplanetary medium — magnetic fields — Sun: particle emission — turbulence

1. INTRODUCTION

The nondispersive "dropouts" of energetic ions from about 20 keV nucleon^{-1} to 2 MeV nucleon^{-1} from impulsive solar flares, as recently observed by the *Advanced Composition Explorer* (*ACE*) spacecraft for a large number of impulsive solar events, occur so frequently and over such small scales ($\sim$0.03 AU) that they cannot be attributed to large-scale magnetic discontinuities and instead must be related to the small-scale structure of the interplanetary magnetic field (Mazur et al. 2000). Similar features have also been observed in solar electron bursts (at less than 1.4 keV) by *ACE*, often in coincidence with the ion dropouts (Gosling et al. 2004). The dropouts are generally attributed to filamentation of magnetic connection from small regions of the solar corona to Earth orbit as the filaments convect past the spacecraft at the solar wind speed, an interpretation that is supported by computer simulations based on a random distribution of transverse fluctuations at the Sun (Giacalone et al. 2000), or anisotropic turbulence in the interplanetary medium (independently by Ruffolo et al. [2003] and by Zimbardo et al. [2004] and Pommois et al. [2005]), distinct physical descriptions that are nevertheless mathematically similar (Giacalone et al. 2006).

Recent work has aimed at better theoretical understanding of why the sharp dropouts occur in observations and in various computer simulations, despite observations of rapid lateral diffusion of energetic particles (e.g., McKibben et al. 2001; McKibben 2005), which might be expected to wash out the dropout features. Generally, one expects the persistence of sharp filamentary features not to be compatible with the homogeneous statistical approach employed in fully diffusive field-line transport models (e.g., Jokipii 1966; Matthaeus et al. 1995; Narayan & Medvedev 2001; Maron et al. 2004). Hence, a different approach required. In terms of a two-component (two-dimensional plus slab or "2D+slab") model of interplanetary turbulence, Ruffolo et al. (2003) proposed that those solar energetic particles (SEPs) follow magnetic field lines, some of which are temporarily trapped by the small-scale topology of the two-dimensional (2D) turbulence. (SEP speeds are much greater than the solar wind speed, so the magnetostatic approximation is adequate and turbulent plasma motions are ignored.) The idea is that interplanetary magnetic field lines are populated with SEPs only in a localized source region near the Sun, as is characteristic of impulsive solar flares (Reames 1992). In the 2D+slab model of solar wind turbulence with no free parameters, some field lines are trapped out to Earth orbit in filaments corresponding to the small-scale topology, that is, islands of closed orbits around O-points in the 2D turbulence (which are filaments in three dimensions), while interstitial field lines spread laterally to large angular distances. This leads to the rapid observation of energetic particles from impulsive solar flares, both in a core region with dropouts and, with lower density, in an extended halo region. Note that in the ensemble average, the field-line random walk is dominated by the 2D component, and field-line diffusion with the diffusion coefficient ($D_\perp$) as calculated or observed (Ruffolo et al. 2003; McKibben 2005) would wash out the sharp dropout features at 1 AU from the Sun that are seen in observations and computer simulations. However, the field lines near O-points undergo little motion due to the 2D turbulence and might be expected to diffuse at a much slower rate, hence the temporary trapping. Thus, traditional ensemble average statistics are not appropriate for describing the dropout phenomenon, and instead we need conditional statistics that depend on the initial location of the field line.

This previous work raises some further issues. If field lines are temporarily trapped (in the two lateral dimensions) in islands around O-points, then how exactly is an island defined? This is not merely an issue of definition, because if there is no physical

[1] Department of Physics and Astronomy, University of Delaware, Newark, DE 19716; paeng@bartol.udel.edu, yswhm@bartol.udel.edu.

[2] Department of Physics, Faculty of Science, Mahidol University, Bangkok 10400, Thailand; david_ruffolo@yahoo.com.

[3] Department of Physics, Faculty of Science, Chulalongkorn University, Bangkok 10330, Thailand; jefuka@hotmail.com.

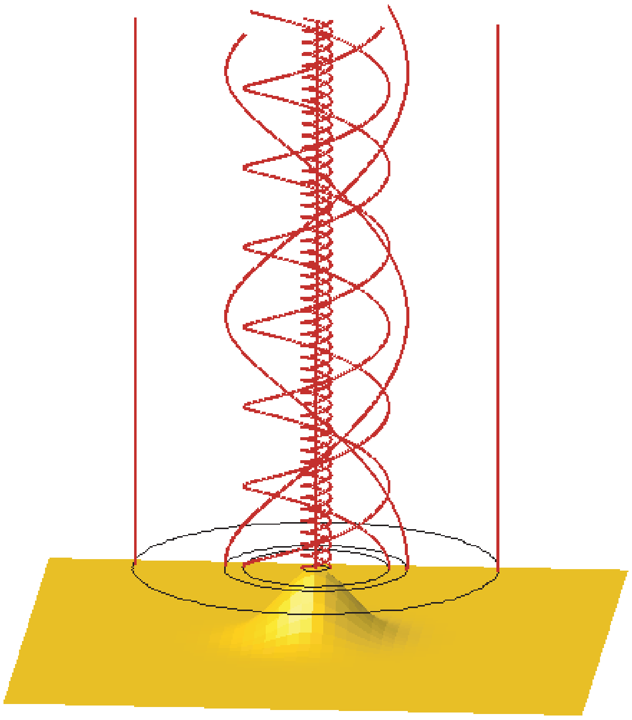

FIG. 1.—Magnetic field line trajectories for a single Gaussian 2D island, with $\boldsymbol{B} = B_0\hat{z} + \boldsymbol{b}^{2D}(x, y)$. In this model system, even with the addition of slab turbulence, field-line trajectories can remain trapped for a particularly long distance with suppressed diffusive escape. The surface plot at bottom shows the potential function $a(x, y)$ of the 2D field.

boundary, it is difficult to understand why the dropouts are so sharp in observations and various simulation models. The islands should not encompass all closed orbits in 2D turbulence, as this would imply too high a filling factor (Kaghashvili et al. 2006). There is also an alternative suggestion that parallel transport of particles along magnetic field lines for intermittent turbulence with certain parameter values could account for the dropout phenomenon (Kaghashvili et al. 2006), though it is yet to be demonstrated that intermittent parallel scattering can produce sharp dropout features as a function of time.

Note that while Ruffolo et al. (2003) expected diffusion within filaments at the slab rate $D_{\rm slab}$, a study of field-line trapping in a single Gaussian 2D magnetic island (a single flux tube; see Fig. 1) with slab turbulence (Chuychai et al. 2005) has demonstrated that the diffusive escape of field lines is in fact suppressed by a strong 2D field and can be much lower than $D_{\rm slab}$. In this system, the suppression effect results in an extended filament of magnetic connection that is unusually resistant to the slab perturbations, apparently enhancing the topological trapping. This further suggests that the actual reason for filamentary magnetic connection to source regions near the Sun is not fully understood.

In the present work, we extend the results of Chuychai et al. (2005) for a single Gaussian 2D island with the 2D field along circular contours (circular "2D orbits"), showing how the trapping length found in computer simulations scales with various parameters and providing an explanation in terms of a quasi-linear theory of the field-line trajectories. We then demonstrate that the suppression mechanism also applies and is even stronger for irregular 2D orbits, with good correspondence between the appropriate quasi-linear theory and computer simulations. Thus, in turbulent 2D+slab fields, since the suppression is most effective where the 2D field is strong, the islands of topological trapping (corresponding to filaments in three dimensions) are sharply delineated by local trapping boundaries, usefully defined by a local maximum in the mean squared field along the 2D orbit. These concepts of temporary trapping by the small-scale topology of 2D turbulence, along with a suppression of the diffusive escape from the trapping regions, can provide a physical explanation of the persistence, sharpness, and intermediate filling factor of dropouts at Earth orbit, as found in both observations and various independent simulation models.

2. TWO-COMPONENT MODEL OF MAGNETIC TURBULENCE

2.1. *Magnetic Field Model*

While some of our results are for a mean field plus a single Gaussian 2D magnetic island (Fig. 1) with the addition of a slab turbulent field, as considered in Chuychai et al. (2005), we also examine field-line trajectories in the full two-component model of magnetic turbulence. This model considers two components of random, transverse fluctuations: a slab component with parallel wavevectors and a 2D component with perpendicular wavevectors. This model has been shown to provide a useful description of magnetic fluctuations in the solar wind (Matthaeus et al. 1990; Bieber et al. 1996) and the transport of energetic particles in the heliosphere, both parallel (Bieber et al. 1994) and perpendicular (Bieber et al. 2004) to the mean magnetic field. It has also been used to classify or estimate various effects of solar wind turbulence, such as the degree of anisotropy at different distances from the Sun (Zank et al. 1996, 1998), in magnetic clouds (Leamon et al. 1998), and in structures of high Alfvén speed (Smith et al. 2001, 2004). Thus, the model is apparently able to encapsulate important features of anisotropic turbulence in the solar wind in a relatively simple mathematical form.

In the 2D+slab model of magnetic field turbulence, we assume

$$\boldsymbol{B} = \boldsymbol{B}_0 + \boldsymbol{b}(x, y, z), \tag{1}$$

where $\boldsymbol{B}_0$ is a uniform mean field in the z-direction and $\boldsymbol{b}$ is the transverse fluctuation ($\boldsymbol{b} \perp \hat{z}$). (Throughout this paper the mean field is always present, so we specify the field model in terms of the fluctuating field $\boldsymbol{b}$.) Here, for simplicity, the magnetic field is static and homogeneous, which means the field does not depend on time and the statistical properties of the magnetic field are invariant under translations. The fluctuation $\boldsymbol{b}$ is perpendicular to the mean field, and $\langle \boldsymbol{b} \rangle$ must be zero. According to the two-component model, the fluctuation in real space can be divided into two parts. In the slab component of turbulence, $\boldsymbol{b}^{\rm slab}$ depends only on z, the coordinate along the mean field, while $\boldsymbol{b}^{2D}$ for the 2D turbulence depends only on the perpendicular coordinates, x and y. Thus, the fluctuation can be written as

$$\boldsymbol{b}(x, y, z) = \boldsymbol{b}^{2D}(x, y) + \boldsymbol{b}^{\rm slab}(z). \tag{2}$$

For the 2D component, we can write

$$\boldsymbol{b}^{2D}(x, y) = \nabla \times a(x, y)\hat{z}, \tag{3}$$

where $a\hat{z}$ is a vector potential for the 2D component and $a(x, y)$ can be called the potential function. From equation (3), one can clearly see that the 2D fluctuation is perpendicular to the gradient of the potential function. Then, for the pure 2D case the field lines must follow level surfaces (contours) of $a(x, y)$, so they are typically trapped on cylinders of finite width (Fig. 1). On the other hand, for pure slab turbulence, the field lines undergo a random walk in (x, y) with correlation length l_c. Therefore, when we combine 2D and slab fluctuations with the mean field, the features of the trapping and random walk of field lines are both found, and either one can dominate depending on where the field lines are initially located (Ruffolo et al. 2003). The two-component model affords great efficiency for computational work. For example, we can reduce the time to generate the turbulent field in the simulations—instead of fully generating it in three dimensions, which requires $N_xN_yN_z$ points to define the three-dimensional fluctuations for calculations, the problem is reduced to using only $N_xN_y + N_z$ points to generate 2D+slab fluctuations.

However, while our goal is to study the magnetic field-line trajectories in real space, both turbulence theory and statistical observations specify the magnetic power spectra of 2D and slab fluctuations in wavevector space. In general, for homogeneous turbulence the magnetic power spectrum $P_{ij}(\boldsymbol{k})$ is defined as the Fourier transform of the magnetic correlation function $R_{ij}(\boldsymbol{r}) = \langle b_i(\boldsymbol{r})b_j(0)\rangle$.

The slab fluctuations in x- and y-components are specified by the magnetic power spectra $P_{xx}^{\rm slab}(k_z)$ and $P_{yy}^{\rm slab}(k_z)$, respectively. The slab fluctuation is then random, depending on z, and is in the direction perpendicular to the mean field. When the slab fluctuation is superposed on the mean field, the field lines wander randomly in space with a correlation length

$$l_c \equiv \frac{\int_0^\infty R_{xx}^{\rm slab}(z)dz}{R_{xx}^{\rm slab}(z=0)} = \sqrt{\frac{\pi}{2}}\frac{P_{xx}^{\rm slab}(k_z=0)}{\langle b_x^2\rangle^{\rm slab}}. \tag{4}$$

According to the relationship in equation (3), the 2D power spectrum can be written in terms of the power spectrum $A(k_x,k_y)$, which is the Fourier transform of the autocorrelation of the potential function $\langle a(x, y)a(0, 0)\rangle$, as

$$P_{xx}^{\rm 2D}(k_x, k_y) = k_y^2 A(k_x, k_y), \tag{5}$$

$$P_{yy}^{\rm 2D}(k_x, k_y) = k_x^2 A(k_x, k_y). \tag{6}$$

In our computer simulations, we need to specify the shape of the spectrum for the turbulent field. Here we choose the Kolmogorov spectrum for both slab and 2D turbulent spectra above the outer scale. For the slab spectrum, we use

$$P_{xx}^{\rm slab}(k_z) = P_{yy}^{\rm slab}(k_z) = \frac{C_1}{[1+(k_zl_z)^2]^{5/6}}, \tag{7}$$

where C_1 is a normalization constant given by

$$C_1 = \sqrt{2\pi}\frac{\Gamma\left(\frac{5}{6}\right)}{\Gamma\left(\frac{1}{2}\right)\Gamma\left(\frac{1}{3}\right)}\langle b_x^2\rangle^{\rm slab} l_z \tag{8}$$

and l_z is a coherence length related to l_c. The spectrum is flat when $k_z \ll 1/l_z$ and rolls over at $k_{0z} = 1/l_z$. For $k_z \gg 1/l_z$, the spectral shape is proportional to $k^{-5/3}$. These features are consistent with observations of solar wind fluctuations (Jokipii & Coleman 1968). For 2D turbulence, we set

$$A(k_\perp) = \frac{C_2}{[1+(k_\perp l_\perp)^2]^{7/3}}, \tag{9}$$

which leads to a 2D spectrum according to equations (5) and (6). Since the 2D omnidirectional power spectrum is proportional to $k_\perp(P_{xx}^{\rm 2D} + P_{yy}^{\rm 2D}) = k_\perp^3 A$, we obtain the Kolmogorov spectrum at $k_\perp \gg 1/l_\perp$. In this 2D magnetic power spectrum, high wavenumbers are associated with small islands of the potential function in real space, whereas low wavenumbers are associated with the large islands. Thus, if we look the surface plot of the turbulent potential function shown in Figure 2, we can see that the topology of 2D turbulence consists of irregular hills and valleys of many sizes. This example shows the topology and field-line random walk for $\langle b^2\rangle^{\rm 2D} = 0.25B_0^2$, $\langle b^2\rangle^{\rm slab} = 0.125B_0^2$, $l_\perp = 0.1$, and $l_z = 1$. It has been suggested that the typical feature size in 2D turbulence is the ultrascale $\tilde{\lambda} = (\langle a^2\rangle/\langle b^2\rangle^{\rm 2D})^{1/2}$ (Matthaeus et al. 1995, 1999), which in this example is 0.0577.

2.2. *Ensemble Average Statistics and Conditional Statistics*

In our numerical simulations, we trace field-line trajectories by solving the field-line equations

$$\frac{dx}{dz} = \frac{b_x^{\rm 2D} + b_x^{\rm slab}}{B_0}, \quad \frac{dy}{dz} = \frac{b_y^{\rm 2D} + b_y^{\rm slab}}{B_0}. \tag{10}$$

These are solved by a fourth-order Runge-Kutta method with adaptive time stepping regulated by a fifth-order error estimate (Press et al. 1992), except where noted otherwise. The magnetic fields are first generated in wavenumber space, and the desired power spectrum is achieved by setting the magnitudes of the complex quantities $b_x(\boldsymbol{k})$ and $b_y(\boldsymbol{k})$ proportional to the square root of the relevant power spectrum. The phases of those quantities are independently random at different $\boldsymbol{k}$-values, and different representations of turbulence can be obtained for different sets of random phases. Then we use an inverse fast Fourier transform to obtain the fluctuating magnetic fields in real space. In our simulations, the turbulent magnetic field is generated (except where noted) over a box of size $L_x = L_y = 40l_z$ and $L_z = 10{,}000l_z$, and the numbers of grid points are $N_x = N_y = 2^{11} = 2048$ and $N_z = 2^{22} = 4{,}194{,}304$. The field lines are traced only to a few percent of the simulation box length in order to avoid periodic effects.

Because of the randomness of the magnetic field, the field lines in the two-component turbulence model undergo a random walk that becomes diffusive at long distances. Calculating the ensemble average of the displacement squared yields the diffusion coefficient of the field lines in the two-component model (Matthaeus et al. 1995) as

$$D_\perp = \tfrac{1}{2}\langle\Delta x^2\rangle/\Delta z = \tfrac{1}{2}D_{\rm slab} + \sqrt{\left(\tfrac{1}{2}D_{\rm slab}\right)^2 + \left(D_{\rm 2D}\right)^2}, \tag{11}$$

where $D_{\rm 2D} = \delta b^{\rm 2D}\tilde{\lambda}/(\sqrt{2}B_0)$ and $D_{\rm slab} = l_c\ \delta b_{\rm slab}^2/(2B_0^2)$. Note that $\delta b^{\rm 2D}$ and $\delta b_{\rm slab}$ denote the rms of the magnetic field in 2D and slab components, respectively. Equation (11) is nonperturbative, and it has been verified by numerical simulations (Gray et al. 1996) over a wide range of fluctuation amplitude. If the 2D component is not present, the diffusion coefficient will be $D_{\rm slab}$ (see Jokipii 1966). Diffusive behavior need not occur in the pure 2D case, because all field lines must follow the contours of constant potential function.

Although the ensemble average field-line random walk is well studied in two-component magnetic turbulence, in actuality each field line wanders differently depending on its (x, y)-location. This leads us to study another kind of statistics in which the initial condition is considered, which we call *conditional statistics* (Ruffolo et al. 2003). From the 2D topology shown as the surface plot in Figure 2, we refer to a local maximum or minimum of $a(x, y)$ as an O-point and a local saddle point of $a(x, y)$ as an X-point. These

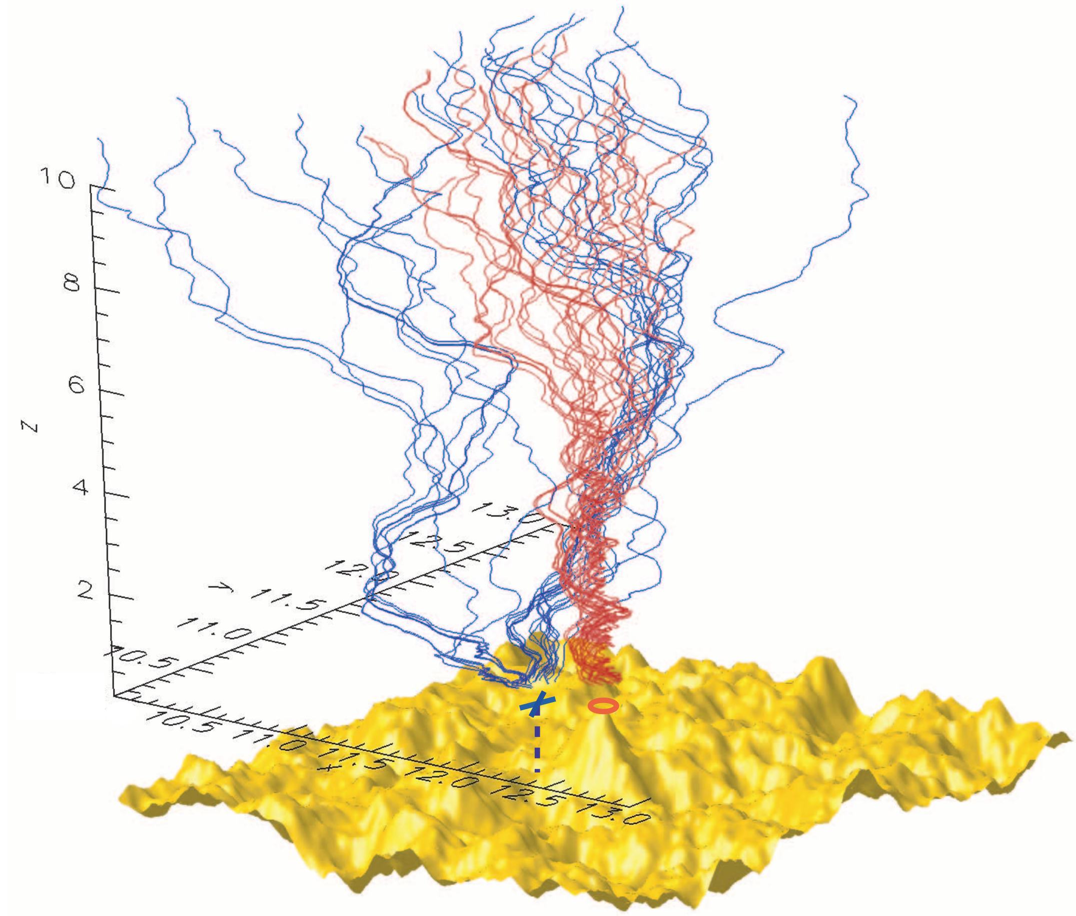

FIG. 2.—Magnetic field line trajectories in a representation of 2D+slab turbulence starting near an O-point (*red*) and an X-point (*blue*). The surface plot at the bottom shows the potential function $a(x, y)$ corresponding to the 2D turbulence.

O- and X-points are special points for $a(x, y)$, and when the slab turbulence is added, the field lines near O-points behave differently from those near X-points. The field lines starting near O-points are temporarily trapped within 2D islands, while they rapidly spread if they start near X-points, as shown in Figure 2. The conditional statistics for this case are demonstrated in Figure 3. We start the field lines near the O-point or the X-point, or at random (x, y)-positions in 2D+slab turbulence, calculating the mean squared displacement and plotting this as a function of distance z. At large z, the mean squared displacement rises linearly for all cases, with diffusion coefficient $D_\perp = 0.0636$, similar to the theoretical value from equation (11) for ensemble average statistics ($D_\perp = 0.0544$). This shows that at large z the distribution of field lines has no "memory" of their initial location; that is, they have spread sufficiently that they sample a wide variety of locations, and the mean squared displacement rises at the same rate. However, there is a varying "delay" at low z, in which the mean squared displacement of field lines starting near an O-point rises more slowly than that for field lines starting near an X-point, because of the temporary trapping of field lines near the O-point. (Note also that the mean squared displacement rises as z^2 in the free-streaming regime at $z \lesssim 1$.) We interpret the delay in z as the trapping length. Then the ensemble average behavior lies between the extremes of starting at an O-point or an X-point.

The characteristics and mechanisms of temporary trapping and escape from the trapping region are explored in the following sections. In § 3, we examine these processes for the simple model system of a mean field plus a single 2D magnetic island plus slab turbulence, including the suppression of diffusive escape from the island for a strong 2D field. In § 4, we then show the connection between the trapping behavior in this model system and in two-component 2D+slab turbulence.

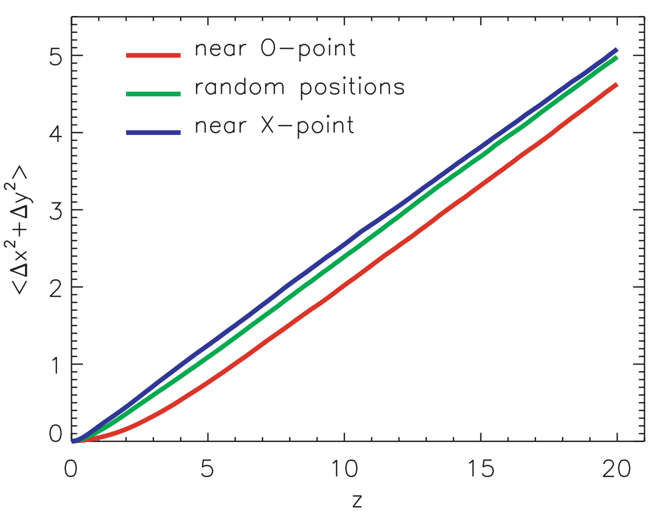

FIG. 3.—Mean squared displacement perpendicular to the mean field for field lines that start near an O-point or an X-point, or at a random position in 2D+slab magnetic turbulence. The delay of the onset of diffusion (the linear rise) demonstrates the trapping effect.

3. FIELD-LINE TRAPPING IN A SINGLE TWO-DIMENSIONAL MAGNETIC ISLAND PLUS SLAB TURBULENCE

3.1. *Magnetic Field Model and Field Lines*

In this section, we use a simple model for the potential function $a(x, y)$ of a single island as a Gaussian function:

$$a(r) = A_0 \exp\left(-\frac{r^2}{2\sigma^2}\right), \quad (12)$$

where A_0 is the maximum value at the center of the island, σ represents the half-width of the Gaussian, and r is measured from the center of the island. The contours of $a(x, y)$ in this case are circles. In the limit of no slab turbulence, the field-line trajectories for $\boldsymbol{B} = B_0\hat{\boldsymbol{z}} + \boldsymbol{b}^{2\mathrm{D}}(x, y)$ have helical orbits along a cylindrical surface of constant $a(x, y)$ with a constant wavenumber (analogous to an angular velocity) $K = a(r_0)/(B_0\sigma^2) = [b^{2\mathrm{D}}(r_0)/B_0]/r_0$, where r_0 is the starting radius as shown in Figure 1. From equation (3), we can write

$$\boldsymbol{b}^{2\mathrm{D}}(r) = \frac{ra(r)}{\sigma^2}\hat{\boldsymbol{\theta}}. \quad (13)$$

The magnitude of $\boldsymbol{b}^{2\mathrm{D}}(r)$ is

$$b^{2\mathrm{D}}(r) = \frac{ra(r)}{\sigma^2} = \frac{rA_0}{\sigma^2}\exp\left(-\frac{r^2}{2\sigma^2}\right), \quad (14)$$

where $b^{2\mathrm{D}}(r)$ has a maximum value at $r = \sigma$, that is, $b^{\max}_{2\mathrm{D}} = A_0/(\sqrt{e}\sigma)$. In general, we set $\boldsymbol{b}^{\mathrm{slab}}$ as described in § 2.1, and we use equations (1) and (2) to specify $\boldsymbol{B}$.

Figure 4 shows an example of two field-line trajectories in a Gaussian 2D field plus slab turbulence. Here the peak of the 2D field is at (10, 10), $\sigma = 0.5$, and $A_0 = 1$. We can see that the field line that starts near the maximum point of the Gaussian (the center of the island) is temporarily trapped with nearly circular orbits within the 2D island. Later, the field line escapes from the 2D island and becomes irregular as a result of the slab turbulence. On the other hand, the field line that starts outside the island simply undergoes a random walk due to slab turbulence. The behavior of the field lines in this simple model are analogous to those of the turbulent system, except that the 2D turbulence contains many 2D islands, including noncircular ones, of many different sizes.

3.2. *Suppressed Diffusion*

When the 2D field is much stronger than the slab component, we can analytically calculate the diffusion rate in the radial direction by using a quasi-linear approach (Chuychai et al. 2005). We take the orbits of field lines to be approximately circular with angular velocity K and treat the slab fluctuation as a perturbation. Therefore, the mean squared displacement in the radial direction is

$$\langle \Delta r^2 \rangle = \frac{1}{B_0^2}\int_0^{\Delta z}\int_0^{\Delta z}\langle b_r^{\mathrm{slab}}(z')b_r^{\mathrm{slab}}(z'')\rangle dz'\,dz'', \quad (15)$$

where $b_r^{\mathrm{slab}}(z)$ is the projection of the slab field in the radial direction, which changes during the circular motion. In terms of the slab correlation function $R_{xx}^{\mathrm{slab}}(\Delta z')$, with $\Delta z' \equiv z'' - z'$ and assuming axisymmetry so that $R_{xx}^{\mathrm{slab}} = R_{yy}^{\mathrm{slab}}$, we have

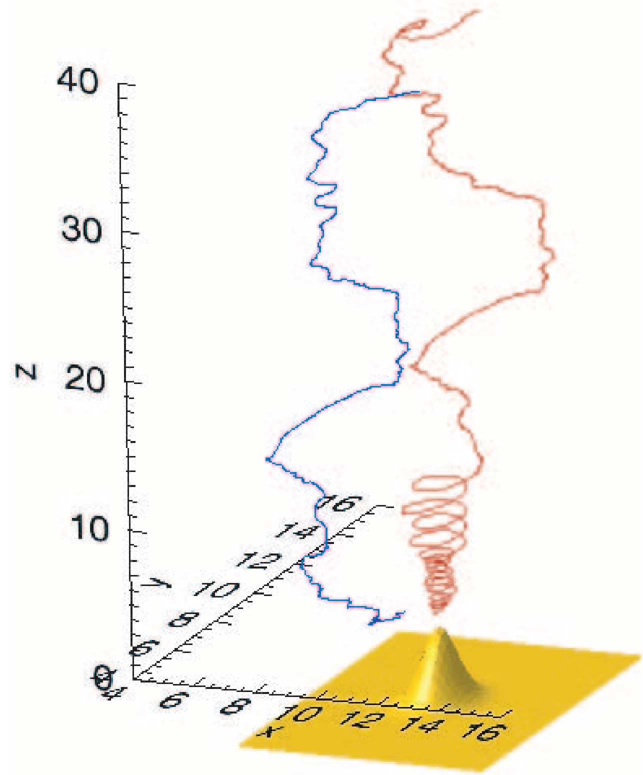

FIG. 4.—Example of two magnetic field lines in a single 2D Gaussian island plus slab turbulence. The red field line started deep inside the island, whereas the blue field line was initially located outside the island. The surface plot at bottom shows the potential function $a(x, y)$ of the 2D field.

$$\langle \Delta r^2 \rangle = \frac{1}{B_0^2}\int_0^{\Delta z}\int_{-\infty}^{\infty} R_{xx}^{\mathrm{slab}}(\Delta z')\cos(K\Delta z')d\Delta z'\,dz', \quad (16)$$

where the integration over all $\Delta z'$ is a valid approximation when $\Delta z \gg l_c$. Rewriting equation (16) in terms of the slab power spectrum $P_{xx}^{\mathrm{slab}}(k_z)$,

$$\langle \Delta r^2 \rangle = \frac{1}{\sqrt{2\pi}B_0^2}\int_0^{\Delta z}\int_{-\infty}^{\infty}\int_{-\infty}^{\infty} P_{xx}^{\mathrm{slab}}(k_z)e^{-ik_z\Delta z'} \times \cos(K\Delta z')dk_z\,d\Delta z'\,dz'. \quad (17)$$

Integrating over $\Delta z'$, k_z, and z', respectively, we have

$$D_{rr} = \frac{\langle \Delta r^2 \rangle}{2\Delta z} = \sqrt{\frac{\pi}{2}}\frac{P_{xx}^{\mathrm{slab}}(K)}{B_0^2} = D_{\mathrm{slab}}\frac{P_{xx}^{\mathrm{slab}}(K)}{P_{xx}^{\mathrm{slab}}(0)}. \quad (18)$$

The theoretical result in equation (18) tells us that radial motion of the field lines deep inside the 2D island is diffusive and is associated with the slab power spectrum at the wavenumber that is resonant with the 2D angular velocity at the original radius. Note that the power spectrum of slab turbulence is typically expected to decrease with increasing k_z, as found in observations of solar wind fluctuations (Jokipii & Coleman 1968) and as in the spectrum we use for simulations (eq. [7]). Indeed, if the correlation function $R_{xx}^{\rm slab}(z)$ is positive and monotonically decreasing, then $P_{xx}^{\rm slab}(0) > P_{xx}^{\rm slab}(K)$ for any $K \neq 0$. Thus, the random walk occurs at a slower rate than it should in slab turbulence. Therefore, we refer to the diffusive behavior in equation (18) as *suppressed diffusion*. The suppression of diffusion arises because the rapid motion around circular orbits effectively decorrelates the radial component of the slab field. The radial coordinate of the field lines increases at the slower rate until they leave the 2D island. Thereafter the diffusion coefficient tends to the slab rate. This theoretical result has already been confirmed by numerical simulations (see Chuychai et al. 2005).

3.3. *Trapping Length and Trapping Boundary*

We note from Ruffolo et al. (2003) that the field lines near O-points in two-component turbulence are trapped within sharp boundaries at intermediate distances, and subsequently all field lines become diffusive. Similar sharp features are seen in observations (Mazur et al. 2000; Gosling et al. 2004) and simulations of particle motion (Giacalone et al. 2000; Zimbardo et al. 2004; Pommois et al. 2005) in turbulent fields. Therefore, we aim to understand over what distance the field lines are trapped, and whether there are sharp trapping boundaries, for the simple model of a single Gaussian 2D island plus slab turbulence.

We perform numerical simulations to examine the parameters that affect the trapping length and trapping boundary. For these simulations, we generate 10,000 field lines in each Gaussian 2D field plus slab turbulence and compute the spread of field lines in space as defined by the function $\Delta R(z) = R(z) - R(0)$, where

$$R(z) = \langle [x(z) - \bar{x}(z)]^2 + [y(z) - \bar{y}(z)]^2 \rangle \quad (19)$$

and $\bar{x}$ and $\bar{y}$ are the average positions at a given z. We choose this statistic because it directly indicates the spread of the field lines at distance z with respect to their center of spreading. We initially start the field lines at various radii from the center of the island. We expect that field lines starting inside and outside the 2D island should behave differently at the beginning and that at a long distance all field lines will leave the 2D island and diffuse at the slab rate.

In the simulations, we vary parameters of the 2D Gaussian island and slab turbulence to explore the effect of their strengths and length scales on the field-line trapping. In Figure 5, we set $b_{\rm 2D}^{\rm max}/B_0 = 2.43$, $\sigma = 0.5$, $l_z = 1.0$, and $\delta b_{\rm slab}/B_0 = 0.5$ and vary the starting radius of the field lines. From the results, we find that when starting deep inside the island, the diffusion of field lines systematically changes, with a delay at the beginning due to the strong 2D field. In contrast, field lines starting outside the boundary immediately diffuse at the slab rate, as shown in Figure 5 (*top*). Here, there are two length scales that we are interested in: the trapping boundary r_c and maximum trapping length $L_{\rm trap}^{\rm max}$, which are calculated from $L_{\rm trap}$ for each initial radius. To evaluate these, we trace the straight line at long z in the $\Delta R(z)$ plot, where it reflects the slab rate of diffusion, and find the z-intercept $L_{\rm trap}$ for each initial radius r_0. Next we plot $L_{\rm trap}$ as a function of r_0 and then fit the low-r_0 portion to a straight line. The $L_{\rm trap}$ intercept is identified as $L_{\rm trap}^{\rm max}$ and the r_0 intercept is called r_c, as illustrated in Figure 5 (*bottom*).

Table 1 shows the derived values of $L_{\rm trap}^{\rm max}$ and r_c for varying magnetic field parameters σ, l_z, $b_{\rm 2D}^{\rm max}/B_0$, and $\delta b_{\rm slab}/B_0$. (Note that the units of length are held fixed, while l_z is allowed to vary.) With additional simulations, the present analysis is more comprehensive than that of Chuychai et al. (2005). When we vary the field parameters, $L_{\rm trap}^{\rm max}$ also changes and can be fitted well with power-law relations as shown in Figure 6. Then we can simply estimate $L_{\rm trap}^{\rm max}$ as

$$L_{\rm trap}^{\rm max} \approx 1.58 l_z^{0.67} \sigma^{0.33} \left[\left(\frac{B_0}{\delta b_{\rm slab}} \right)^2 \right]^{1.1} \left(\frac{b_{\rm 2D}^{\rm max}}{B_0} \right)^{1.64}. \quad (20)$$

From Table 1, we can see that $r_c \sim \sigma$, depending only weakly on other parameters.

We can explain the behavior of the length scales $L_{\rm trap}^{\rm max}$ and σ with suppressed-diffusion theory. From equation (18), we can see that the diffusion coefficient of field lines in the radial direction, D_{rr}, depends on the power spectrum at the wavenumber $k_z = K$ that resonates with the angular frequency of 2D field lines of starting radius r_0. For K-values in the energy-containing range ($K \lesssim 1/l_z$) and the inertial range ($K \gtrsim 1/l_z$) of the power spectrum of slab turbulence, we can obtain very different values of D_{rr}. We have $K \lesssim 1/l_z$ for field lines that start at low effective angular frequency $K = b^{\rm 2D}(r_0)/r_0$ (e.g., outside the 2D island), and in this case $P_{xx}^{\rm slab}(K) \approx P_{xx}^{\rm slab}(0)$. Thus, field lines starting outside the island should diffuse at the slab rate. On the other hand, we have $K \gtrsim 1/l_z$ for field lines that start at high angular frequency, inside a sufficiently strong 2D island. At these higher k_z-values we have a Kolmogorov spectrum, $P_{xx}^{\rm slab} \propto k_z^{-5/3}$. The field lines in this region spread at the suppressed diffusive rate; that is, they are temporarily trapped within the 2D island. Thus, the trapping boundary should correspond to r_c such that

$$l_z K(r_c) \sim 1, \quad (21)$$

where the power spectrum of slab turbulence rolls over.

For the specific form of a Gaussian 2D island, we use $K = a(r)/(B_0 \sigma^2)$ and $a(r) = A_0 \exp[-r^2/(2\sigma^2)]$, so K monotonically decreases with radius r. Thus, the suppression effect is strongest for the highest K-values at the center of the island. The condition for the trapping boundary, equation (21), becomes

$$1 \sim \frac{A_0 \exp(-r_c^2/2\sigma^2) l_z}{B_0 \sigma^2}, \quad (22)$$

$$r_c \sim \sqrt{2\sigma^2 \ln\left(\frac{A_0 l_z}{B_0 \sigma^2} \right)}. \quad (23)$$

The maximum value of the 2D field is $A_0/(\sqrt{e}\sigma)$ at $r = \sigma$. Substituting $A_0 = \sqrt{e}\sigma b_{\rm 2D}^{\rm max}$ into equation (23), we have

$$r_c \sim \sigma \left[1 + \ln\left(\frac{b_{\rm 2D}^{\rm max} l_z}{B_0 \sigma} \right)^2 \right]^{1/2}. \quad (24)$$

Equation (24) shows that r_c is on the order of σ, with only a weak dependence on other parameters, since the ratio $b_{\rm 2D}^{\rm max} l_z/(B_0 \sigma)$ appears in the natural logarithm.

Since the field lines are trapped most effectively when they are initially located at the center of the Gaussian island, we next consider the maximum trapping length along the mean field direction. If we start at $r_0 = 0$ and want to estimate the Δz over which the radius reaches the trapping boundary r_c, then from $\Delta r^2 = 2D_{rr}\Delta z$,

$$r_c^2 \sim D_{rr} L_{\rm trap}^{\rm max} \sim \frac{P_{xx}^{\rm slab}(K)}{B_0^2} L_{\rm trap}^{\rm max}. \quad (25)$$

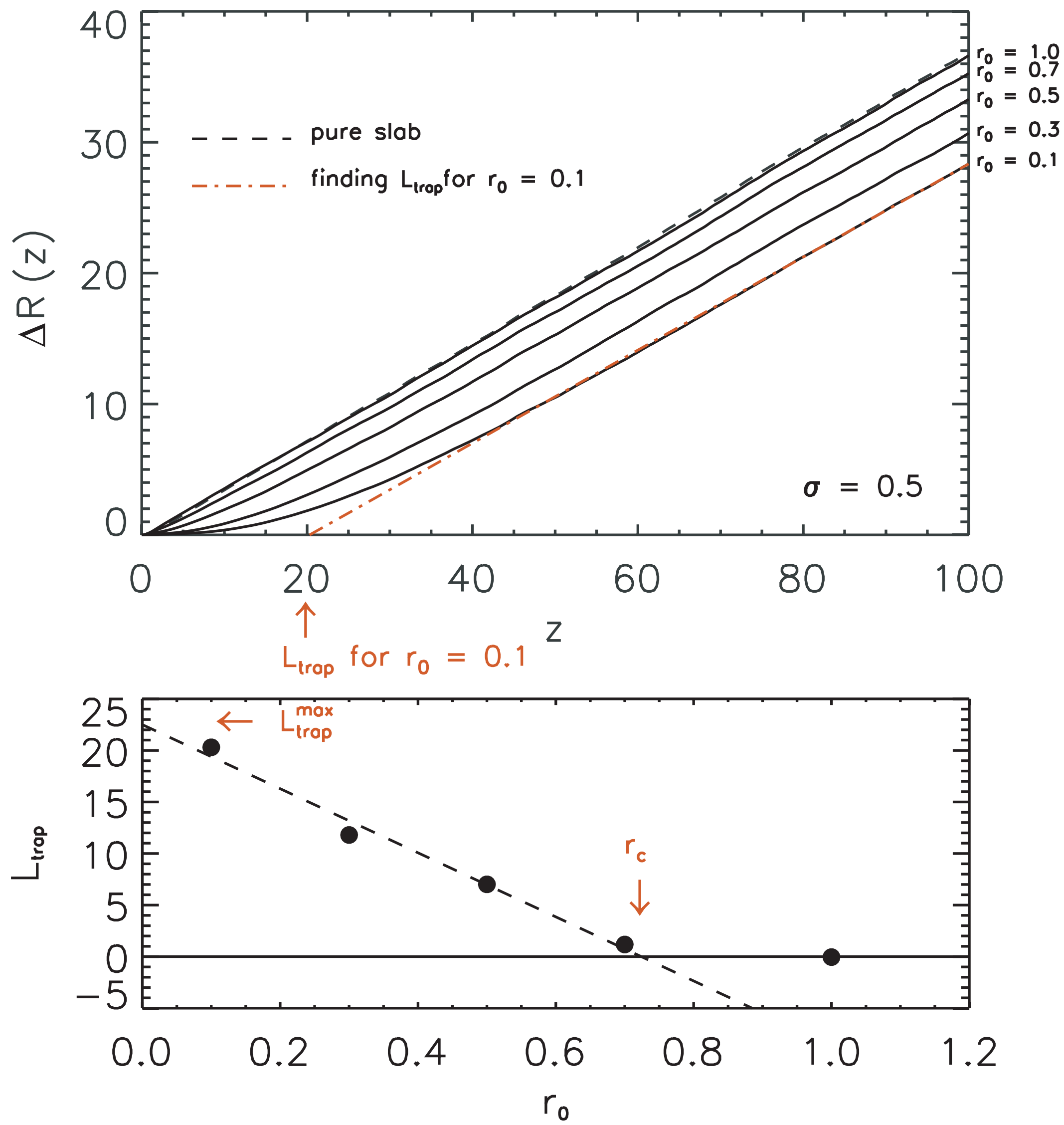

FIG. 5.—*Top*: Spreading function ΔR of magnetic field lines in a single 2D island plus slab turbulence, as a function of distance z along the mean field, for varying initial distance r_0 from the island center. The definition of the trapping length $L_{\rm trap}$ is illustrated for the case of $r_0 = 0.1$. *Bottom*: Plot of $L_{\rm trap}$ as a function of r_0, illustrating the definition of the maximum trapping length $L_{\rm trap}^{\rm max}$ and the trapping boundary r_c.

TABLE 1

FIELD-LINE TRAPPING PARAMETERS $L_{\rm trap}^{\rm max}$ AND r_c FOR A SINGLE TWO-DIMENSIONAL MAGNETIC ISLAND WITH SLAB TURBULENCE

	Run Parameters				Fit Parameters	
Run	$b_{2D}^{\rm max}$	σ	$\delta b_{\rm slab}$	l_z	$L_{\rm trap}^{\rm max}$	r_c
1..............	0.607	0.5	0.5	1.0	2.66	0.76
2..............	1.82	0.5	0.5	1.0	15.59	0.56
3..............	2.43	0.5	0.5	1.0	22.50	0.72
4..............	6.07	0.5	0.5	1.0	121.53	0.72
5..............	6.07	0.5	1.12	1.0	19.59	0.66
6..............	6.07	0.5	1.58	1.0	9.31	0.77
7..............	6.07	0.5	0.5	0.7	94.35	0.72
8..............	6.07	0.5	0.5	0.5	73.34	0.78
9..............	6.07	0.5	0.5	0.3	54.39	0.82
10............	2.43	0.9	0.5	0.3	27.27	1.76
11............	2.43	0.7	0.5	0.3	25.57	1.02
12............	2.43	0.3	0.5	0.3	18.30	0.38

Therefore,

$$L_{\rm trap}^{\rm max} \sim r_c^2 B_0^2 / P_{xx}^{\rm slab}(K). \qquad (26)$$

Since r_c is on the order of σ,

$$L_{\rm trap}^{\rm max} \sim \sigma^2 B_0^2 / P_{xx}^{\rm slab}(K). \qquad (27)$$

For high k_z, we use a Kolmogorov spectrum for slab turbulence as specified by equations (7) and (8). Therefore, for $l_z K \gg 1$

$$P_{xx}^{\rm slab}(K) \sim \delta b_{\rm slab}^2 l_z (K l_z)^{-5/3}. \qquad (28)$$

Rewriting K in terms of $b_{2D}^{\rm max}/B_0$ and σ, we have

$$P_{xx}^{\rm slab}(K) \sim \delta b_{\rm slab}^2 l_z \left(\frac{B_0 \sigma}{b_{2D}^{\rm max} l_z} \right)^{5/3}. \qquad (29)$$

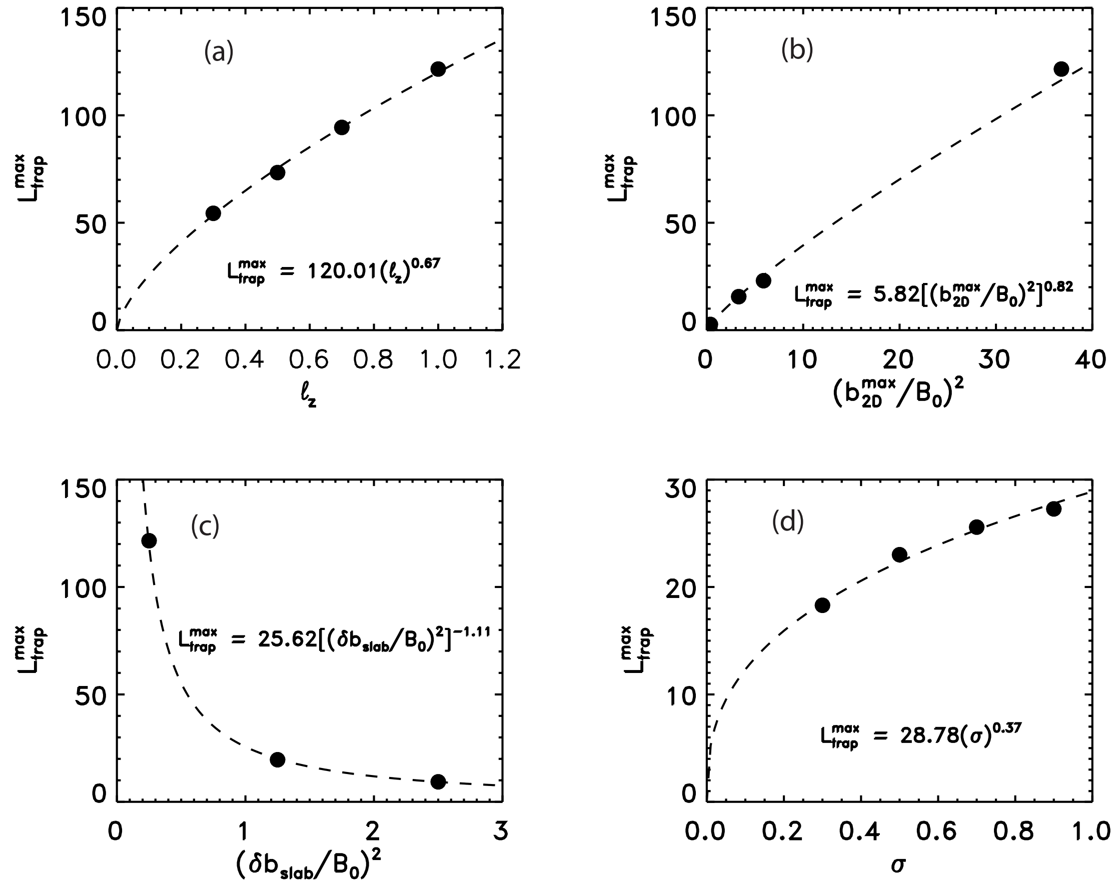

FIG. 6.—Power-law fits of $L_{\rm trap}^{\rm max}$ as a function of (*a*) l_z, (*b*) $(b_{\rm 2D}^{\rm max}/B_0)^2$, (*c*) $(\delta b_{\rm slab}/B_0)^2$, and (*d*) σ.

Therefore, the maximum of trapping length in equation (27) can be scaled as

$$L_{\rm trap}^{\rm max} \sim \sigma^{1/3} l_z^{2/3} \left(\frac{B_0}{\delta b_{\rm slab}}\right)^2 \left(\frac{b_{\rm 2D}^{\rm max}}{B_0}\right)^{5/3}. \tag{30}$$

The theoretical scaling for $L_{\rm trap}^{\rm max}$ in equation (30) is very close to the power-law fit that we find from the simulations (eq. [20]). We can see that the trapping length depends on the length scales of the 2D and slab fields, is nearly proportional to the peak 2D field energy, and inversely depends on the slab turbulent energy. Since (for a Gaussian flux tube) the 2D field is strongest at σ, it seems that the field lines are trapped within the region where the 2D field is strongest, which leads to the trapping boundary. Even a 2D island of small size can trap the field lines if the maximum 2D field is sufficiently strong, for appropriate values of the other parameters.

4. FIELD-LINE TRAPPING IN 2D+SLAB MAGNETIC TURBULENCE

With the results of the previous section, we now have a mechanism to explain the sharpness and persistence of field-line trapping in a 2D magnetic island over a long distance, as found in observations and simulations of the dropout phenomenon. The mechanism by which field lines escape from the island is diffusive, but in addition to the topological effect that removes the 2D contribution to diffusion near O-points in a turbulent 2D field (Ruffolo et al. 2003), we see that a strong 2D field can also suppress the diffusive escape due to slab turbulence.

Does the mechanism of suppressed diffusive escape apply to solar wind turbulence? The solar wind indeed has a strong 2D component, estimated to account for 80% to 85% of the turbulent energy (Bieber et al. 1994, 1996), though this is not as overwhelmingly strong as the values used for simulations in § 3. Another difference is that the Gaussian 2D island used in § 3 has an angular velocity $b^{\rm 2D}/r$ that has a maximum value and is roughly constant at the center of the island. That specific condition may not apply to turbulent 2D islands. Turbulent 2D islands are not circular, so a "radius" is not defined, and there are many islands of different sizes, many of which are nested. A theoretical concern is how to define an "island" or a topological region "near an O-point," perhaps in terms of a trapping boundary as in § 3.

In this section, we are able to address all these concerns and confirm that suppressed diffusive escape indeed does apply to the turbulent 2D+slab model, which captures many of the important features of solar wind turbulence. In § 4.1, we generalize the theory of suppressed diffusion to noncircular 2D orbits and confirm the theory with numerical simulations. To achieve this with irregular turbulent islands, it is necessary to formulate the theory in terms of the potential function. We find that quantifying the parameters of the trapping and escape processes is made considerably more difficult by the random structure of the 2D field; nevertheless, in § 4.2 we examine the ideas of the trapping length and maximum extent of the trapping (now in potential rather than radius). Although we find that a consistent picture emerges for isolated islands, we seek a formulation that helps identify possible trapping structures without the need to first compute statistics of many field lines. To this end, in § 4.3 we introduce the idea of "local trapping boundaries" and discuss how the interplay between 2D flux structures and 2D magnetic field strength leads to the likelihood of trapping.

4.1. *Suppressed Diffusion*

The picture of trapping and suppressed diffusive escape that we found in the context of a single Gaussian island in the presence of slab turbulence is satisfying only if we can extend it in a meaningful way to the case of random 2D islands that provide trapping and, again (for simplicity), slab turbulence to induce the escape of field lines. The general problem is complicated by the fact that escape from one island may or may not lead to subsequent capture by nearby 2D flux structures and, therefore, the necessity of dealing with the statistics of 2D islands rather than an individual structure. Here, to avoid that complication we extend the earlier calculation of suppressed diffusive escape by again considering a single 2D flux structure, but one that allows for arbitrary contours of the associated field line. We will consider only closed 2D field lines, and we again work in the context of a quasi-linear formulation.

Consider the slab fluctuations as perturbations to a 2D orbit $(X(z), Y(z))$ that is a simply connected equipotential contour, with a complete orbit traversed over a finite distance Z along the mean field. This implies that there are no neutral points ($\boldsymbol{b}^{2\mathrm{D}} = 0$) along the closed 2D field line. In general these 2D orbits are not circles, in contrast to § 3. Nevertheless, we can apply quasi-linear theory to explain the suppression of slab diffusion. Though the radius r is not well defined, we can instead interpret Δr as motion perpendicular to the unperturbed 2D orbit. Alternatively, we can express the perpendicular motion in terms of Δa, the change in $a(x, y)$. We outline two derivations, for Δr and for Δa.

The derivation for Δr starts as in equation (15):

$$\langle \Delta r^2 \rangle = \frac{1}{B_0^2} \int_0^{\Delta z} \int_0^{\Delta z} \langle b_r^{\mathrm{slab}}(z') b_r^{\mathrm{slab}}(z'') \rangle dz'\, dz''. \quad (31)$$

In this case, the perpendicular component $b_r^{\mathrm{slab}}(z)$ is defined by

$$b_r^{\mathrm{slab}}(z) = b_x^{\mathrm{slab}} c(z) + b_y^{\mathrm{slab}} s(z), \quad (32)$$

where $c(z)$ and $s(z)$ are the direction cosine and sine of a normal to the unperturbed orbit,

$$c(z) \equiv \frac{dY/dz}{\sqrt{(dX/dz)^2 + (dY/dz)^2}},$$
$$s(z) \equiv \frac{-dX/dz}{\sqrt{(dX/dz)^2 + (dY/dz)^2}} \quad (33)$$

with $dX/dz = b_x^{2\mathrm{D}}/B_0$ and $dY/dz = b_y^{2\mathrm{D}}/B_0$. Then from equation (31) we obtain

$$\langle \Delta r^2 \rangle = \frac{1}{B_0^2} \int_0^{\Delta z} \int_{-\infty}^{\infty} [R_{xx}^{\mathrm{slab}}(\Delta z') c(z') c(z' + \Delta z') + R_{yy}^{\mathrm{slab}}(\Delta z') s(z') s(z' + \Delta z')] d\Delta z'\, dz'. \quad (34)$$

Because $c(z)$ and $s(z)$ are periodic with period Z, we can define the Fourier series

$$c(z) = \sum_{n=-\infty}^{\infty} c_n e^{i2\pi nz/Z}, \quad s(z) = \sum_{n=-\infty}^{\infty} s_n e^{i2\pi nz/Z}. \quad (35)$$

Note that $c_{-n} = c_n^*$ and $s_{-n} = s_n^*$ because $c(z)$ and $s(z)$ are real. With the axisymmetry property $R_{xx}^{\mathrm{slab}} = R_{yy}^{\mathrm{slab}}$, we obtain

$$\langle \Delta r^2 \rangle = \frac{\Delta z}{B_0^2} \sum_{n=-\infty}^{\infty} \int_{-\infty}^{\infty} R_{xx}^{\mathrm{slab}}(\Delta z')(|c_n|^2 + |s_n|^2) \times e^{i2\pi n\Delta z'/Z} d\Delta z'. \quad (36)$$

Then

$$D_{rr} = \frac{\langle \Delta r^2 \rangle}{2\Delta z} = \frac{D_{\mathrm{slab}}}{P_{xx}(0)} \sum_{n=-\infty}^{\infty} (|c_n|^2 + |s_n|^2) P_{xx}(nK). \quad (37)$$

For the case of a circular 2D orbit, the above expression indeed reduces to equation (18). We see that for a general 2D orbit, the diffusion coefficient actually depends on the power spectrum at various harmonics nK, weighted according to the Fourier series of the direction cosine and sine for the unperturbed 2D orbit.

For comparison with numerical simulations, it is easier to use a diffusion coefficient in $a(x, y)$, defined by

$$D_{aa} \equiv \tfrac{1}{2} \langle (\Delta a)^2 \rangle / \Delta z. \quad (38)$$

Note that

$$\frac{da}{dz} = b_x^{\mathrm{slab}} C(z) + b_y^{\mathrm{slab}} S(z), \quad (39)$$

where we define

$$C(z) \equiv \frac{dY}{dz}, \quad S(z) \equiv -\frac{dX}{dz}. \quad (40)$$

By analogy with the previous derivation, we use Fourier amplitudes C_n and S_n defined by

$$C(z) = \sum_{n=-\infty}^{\infty} C_n e^{i2\pi nz/Z}, \quad S(z) = \sum_{n=-\infty}^{\infty} S_n e^{i2\pi nz/Z}. \quad (41)$$

We then obtain

$$D_{aa} = \frac{D_{\mathrm{slab}} B_0^2}{P_{xx}(0)} \sum_{n=-\infty}^{\infty} (|C_n|^2 + |S_n|^2) P_{xx}(nK). \quad (42)$$

This expression is more convenient mathematically, because of the simpler definitions of $C(z)$ and $S(z)$. By Parseval's theorem,

$$\sum_{n=-\infty}^{\infty} (|C_n|^2 + |S_n|^2) = \langle C^2 + S^2 \rangle = \frac{\langle b^2 \rangle^{2\mathrm{D}}}{B_0^2}. \quad (43)$$

Note that $C_0 = S_0 = 0$ because the closed 2D orbit implies that dX/dz and dY/dz integrate to zero over one period. Thus indeed we could write

$$D_{aa} = \frac{D_{\mathrm{slab}} B_0^2}{P_{xx}(0)} \sum_{\substack{n=-\infty \\ n\neq 0}}^{\infty} (|C_n|^2 + |S_n|^2) P_{xx}(nK). \quad (44)$$

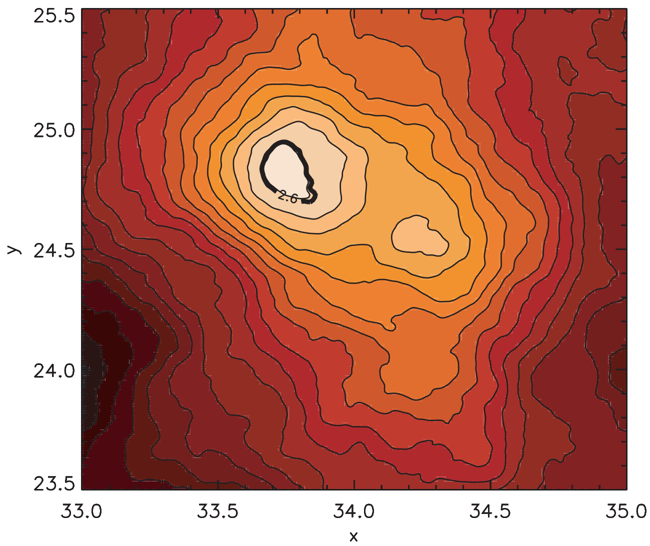

FIG. 7.—Contour plot of $a(x, y)$ for a representation of 2D turbulence used for verification of the suppressed-diffusion theory for a noncircular contour. The heavy curve indicates the 2D orbit where the field lines start.

Now compare this contour with an equivalent circular contour of the same $\langle b^2\rangle^{2D}$, in which the entire sum in equation (44) is concentrated at $n = \pm 1$. If $P^{\rm slab}_{xx}(k_z)$ is a monotonically decreasing function, a circular 2D orbit always has the *maximum* diffusion rate D_{aa} of any contour with the same $\langle b^2\rangle^{2D}$. Any noncircular 2D orbit has enhanced suppression over that found in § 3.

This shows that the suppression of slab diffusion applies when $\boldsymbol{b}^{2D}$ is strong *or* the orbit is irregular. Mathematically, for a highly irregular orbit the power spectrum is sampled mainly at higher harmonics nK, leading to a greatly reduced rate of diffusion. Physically, the suppressed diffusion is due to decorrelation of the slab random flights in r, the direction normal to the 2D orbit, by rotation of the normal direction in (x, y)-space. When the orbit is highly irregular, the normal direction rotates rapidly and the normal excursions due to slab random flights decorrelate quickly in z, resulting in low diffusion in the normal direction.

To verify the generalized suppressed-diffusion formula (eq. [44]), we perform numerical simulations of field-line trajectories in 2D+slab turbulence. Note that this theory is a microscopic description, aiming to explain diffusive escape from a single 2D contour, and does not apply to a distribution of field lines spanning many contours. Therefore, for purposes of verifying the theoretical concepts, we use a particularly strong 2D field and a weak slab field so that the distribution spreads slowly enough to allow a measurement of D_{aa}. In addition, quasi-linear ordering, that is, use of unperturbed trajectories as a first approximation, formally requires in this case that the slab turbulence be weak.

We consider an equipotential contour of constant $a(x, y)$ around an O-point in an arbitrarily chosen sample of 2D turbulence that contains a visually well-defined island (Fig. 7). Here the units are l_z along x, y, and z and B_0 for the magnetic field. The magnetic field is generated over $L_x = L_y = 40l_z$ and $L_z = 10{,}000l_z$, and the numbers of grid points are $N_x = N_y = 2^{12} = 4096$ and $N_z = 2^{22} = 4{,}194{,}304$. For demonstration purposes, we choose the size of the 2D island to be $\sim l_z$, and the local maximum rms 2D field along the selected contour is $3.4B_0$, which is located at the level $a(x, y) = 1.85$. The maximum $a(x, y)$ of this island is 2.85. We start 10,000 field lines on the contour that has $a(x, y) = 2.6$ (Fig. 7, *heavy curve*), which is still within the 2D island and close to the O-point. Here we perform six sets of simulations with varying slab energies $\delta b^2_{{\rm slab},x}/B_0^2$ of 0.0005, 0.00125, 0.0025, 0.005, 0.025, and 0.125. We place field lines at random initial locations along the selected contour and then trace the field-line trajectories and calculate D_{aa} as in equation (38) and compare this with the quasi-linear theory in equation (44). To obtain the theoretical value, we analyze the unperturbed trajectory of a field line (for pure 2D fluctuations) at the same contour level where we perform the simulations and find C_n- and S_n-values for that unperturbed trajectory.

Figure 8 illustrates the results for D_{aa} as a function of z from the computer simulations in comparison with the theoretical values from equation (44). In each case the theoretical value of

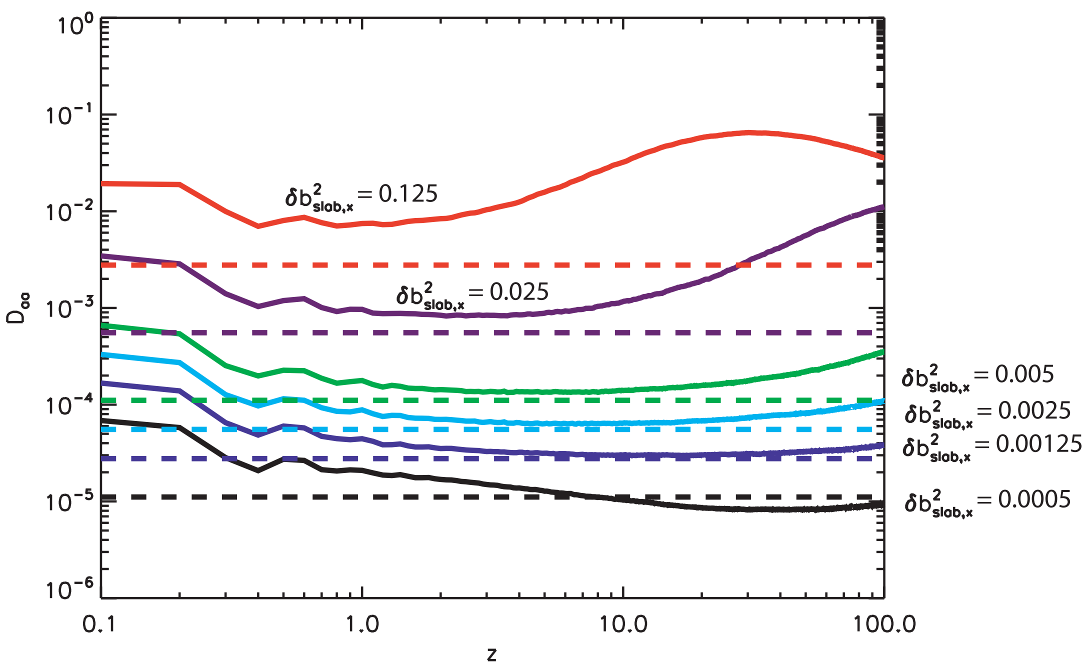

FIG. 8.—Magnetic field line diffusion coefficient D_{aa} in 2D+slab turbulence from simulations (*solid lines*) and theoretical values (*dashed lines*) when $\delta b^2_{{\rm slab},x}$ is varied.

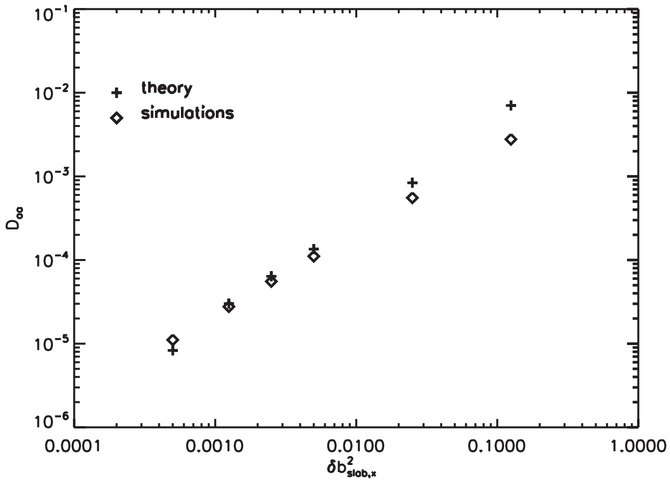

Fig. 9.—Comparison between simulations and theory for the suppressed-diffusion coefficient D_{aa} with varying $\delta b^2_{\mathrm{slab},x}$.

D_{aa} is 168 times lower than the value for pure slab turbulence, indicating significant suppression of slab diffusion. The measurement is somewhat difficult because at $z \lesssim 1$ (i.e., less than a coherence length) the random walk is not yet diffusive, while at long z the distribution of a-values is distorted by its nonlinear dependence on the distance traveled normal to the 2D orbit. Nevertheless, we can recognize that the field-line diffusion is suppressed as a result of the 2D field, as D_{aa} remains nearly constant over $1 \lesssim z \lesssim 10$, near the theoretical value, which is 5.95×10^{-3} of the pure-slab value.

We compare the average value of D_{aa} where the suppressed diffusion occurs and plot it along with the theoretical value from the quasi-linear approach in Figure 9. It is clear that the theory works well when the 2D field is much stronger than the slab turbulence, that is, in the quasi-linear regime. For higher $\delta b^2_{\mathrm{slab},x}$, quasi-linear theory is expected to fail, and in addition, it is difficult to accurately measure D_{aa}, as the field lines rapidly leave the initial contour.

4.2. *Local Trapping Length*

We have seen that the suppression of diffusive escape from a trapping region, a concept developed in the context of a single 2D magnetic island (Chuychai et al. 2005), can successfully be generalized to fluctuating 2D fields and is even more effective for irregular 2D orbits. We now demonstrate that the concepts of the trapping length and maximum extent of trapping, developed in § 3.3 for a single 2D magnetic island, also apply to fluctuating fields.

In this section, we use simulation parameters similar to solar wind conditions, as in Ruffolo et al. (2003), in particular using $\delta b/B_0 = 0.5$, a 2D-to-slab energy ratio of 80 : 20, a slab correlation length $l_c = 0.02$ AU, and an ultrascale of $\tilde{\lambda} = 0.06$ AU. The magnetic field is generated in a simulation box with $L_x = L_y = 100 l_z$, $L_z = 1000 l_z$ and $N_x = N_y = 2^{11} = 2048$, $N_z = 2^{22} = 4{,}194{,}304$. Since there are many islands in 2D turbulence, here we select only one 2D turbulent island to explore the diffusion of field lines that start at different levels $a(x, y)$ in that local island. The contour plot of $a(x, y)$ of the island that we choose is shown in Figure 10 at upper left. We pick five levels of $a(x, y)$, and 10,000 field lines initially start on each level. The trajectories of field lines are traced until 20 AU. Now the island has an irregular shape and is not symmetric around the center of the island, so it is hard to use statistics like those in § 3.3. Therefore, the statistic that we use for field lines in this section is the mean squared displacement perpendicular to mean field ($\langle \Delta x^2 + \Delta y^2 \rangle$) as presented in Figure 3. The plot of $\langle \Delta x^2 + \Delta y^2 \rangle$ as a function of distance Δz is illustrated in Figure 10. One can see behavior similar to that shown in § 3.3. That is, the field lines have a delayed spread at small distances and later they approach diffusive behavior. However, instead of slab diffusion, here we obtain the diffusion coefficient for the two-component model (eq. [11]). The same procedure as in § 3.3 is used in order to find L_{trap} for the 2D turbulent island. The inset at bottom right in Figure 10 shows the L_{trap} of the field lines for each level of $a(x, y)$. Thus, if we simply use linear least-squares fitting to determine the maximum trapping and a boundary analogous to the definition of r_c in § 3.3, which here we call a_c, we find $L_{\mathrm{trap}}^{\max} = 5.36$ AU at the maximum of $a(x, y)$ of this island and $a_c = 0.35$ in units of $B_0 l_z$. (Note that the new method to find trapping boundaries that we present in § 4.3 gives the local trapping boundary for this case at $a = 1.29$.) It is difficult to see clearly in the contour plot of $a(x, y)$ whether this boundary is the trapping boundary, because this a_c-level is located almost at the edge of the island, and if we go further than this, there are other islands. Therefore, we consider another definition of a trapping boundary that might work better than a_c. In the next subsection, we present a new idea to define trapping boundaries of 2D turbulence structures that depend on only the properties of the 2D field, without knowledge of the statistics of the field-line random walk.

4.3. *Local Trapping Boundaries*

In this section, we synthesize the concepts developed in previous sections to explain the sharp, persistent boundaries of magnetic connection that correspond to dropout features. The dropout phenomenon can be attributed to the filamentary distribution of magnetic connection to a small region near the Sun, that is, the region where an impulsive solar flare injects particles onto interplanetary magnetic field lines. (We note in passing that the physical mechanism or mechanisms by which particles escape the flare region are not entirely clear.) For numerical simulations, we select a representation of 2D+slab magnetic turbulence as specified in § 2.1. We then trace magnetic field lines from random positions within the injection region, a circle at $z = 0$, and plot the locations of the field lines in the (x, y)-plane at various distances z. In this case the field-line tracing was performed by a slightly different technique. Inside an individual cell defined by Fourier transform grid points, the field-line equations (eq. [10]) are solved analytically for a bilinear interpolation of the potential function $a(x, y)$ and a linear interpolation of the slab magnetic field, a method developed by P. Pongkitiwanichakul et al. (2007, in preparation). We use simulation parameters similar to solar wind conditions, as in Ruffolo et al. (2003), in particular by taking $\delta b/B_0 = 0.5$, a 2D-to-slab energy ratio of 80 : 20, a slab correlation length $l_c = 0.02$ AU, and an ultrascale of $\tilde{\lambda} = 0.06$ AU. The magnetic field is generated in a simulation box with $L_x = L_y = 100 l_z$, $L_z = 1000 l_z$ and $N_x = N_y = 2^{11} = 2048$, $N_z = 2^{22} = 4{,}194{,}304$.

As an example, consider the contour plot of the potential function $a(x, y)$ of a representation of 2D turbulence as shown in Figure 11 and the corresponding scatter plots of field-line locations in (x, y) at various z (Fig. 12). There are sharp boundaries to regions of temporary trapping of field lines. We seek a mathematical prescription to identify such boundaries. Since the field-line motion in (x, y) is dominated by the 2D field, which lies along contours of constant $a(x, y)$, a local trapping boundary should lie along such a contour. Note also that the red shading in Figure 12 shows $b^2_{\mathrm{2D}}(x, y)$, and in many cases the sharp gradients in the density of field lines correspond to regions of strong b^2_{2D}.

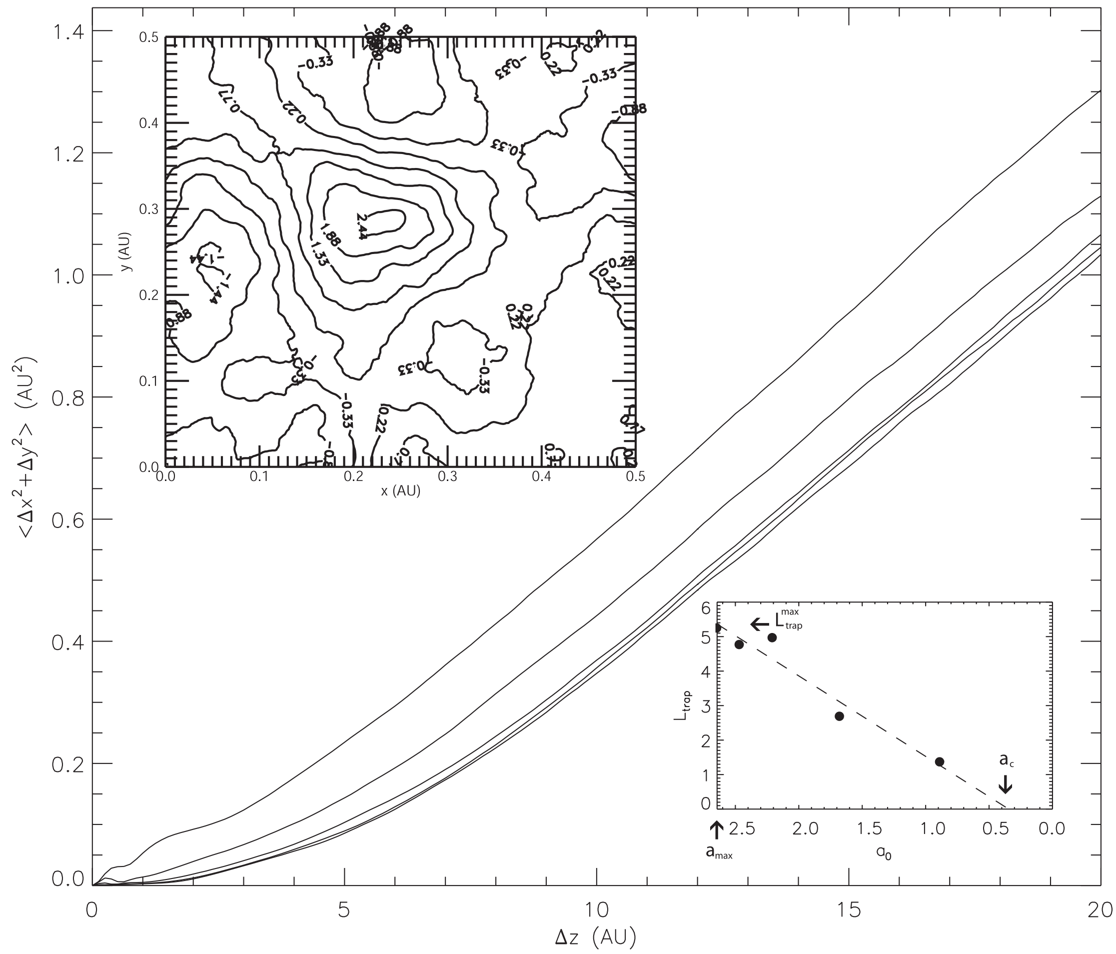

FIG. 10.—Mean squared displacement perpendicular to the mean field for field lines that start at five different levels of the selected local 2D island (*inset, upper left*). $L_{\rm trap}^{\rm max}$ of each level and the linear least-squares fit are shown at lower right.

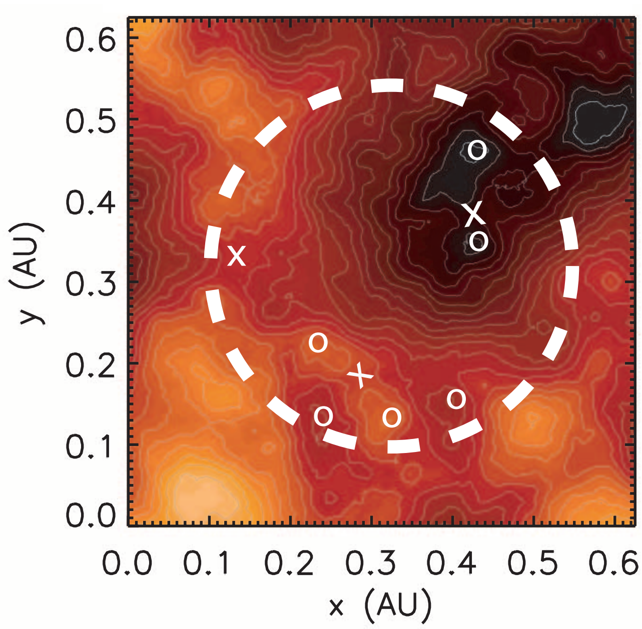

FIG. 11.—Contour plot of $a(x, y)$ for a representation of 2D turbulence, indicating O-points and X-points. Near O-points, the 2D turbulence contributes little to the field-line transport in (x, y) as a function of z.

Therefore, we consider the mathematical prescription of a local trapping boundary (LTB) as an equipotential contour that has a maximum average 2D fluctuation energy when compared with neighboring contours. More specifically, we use the average value of $|b^{\rm 2D}|^2$ along the equipotential contour,

$$|b^{\rm 2D}|^2_{\rm av} = \frac{1}{L}\int |b^{\rm 2D}(x,y)|^2 dl, \qquad (45)$$

where dl is an element of arc length along the contour (in the x-y plane) and L is the total length of the contour. The results in this section are obtained from searches for maximum values of $|b^{\rm 2D}|^2_{\rm av}$, starting from various trial locations. We also tried a similar prescription replacing the average over dl with an average over dz, with little difference in the results.

LTBs determined according to equation (45) are shown as solid lines in Figure 12. The mathematical prescription for LTBs indeed corresponds closely to persistent sharp gradients in the concentration of field lines that started in the same circle at $z = 0$. Some LTBs visually correspond to an island of trapping around a cluster of O-points, but many do not. It is interesting that the LTBs organize the field-line connectivity much better than "regions around O-points" (the topology effect alone) or the distribution of $b^2_{\rm 2D}$ (the suppression effect alone). Specific examples are provided below. The LTBs incorporate the concepts of 2D topology and suppressed slab diffusion to effectively describe the field-line trapping and dropout phenomena.

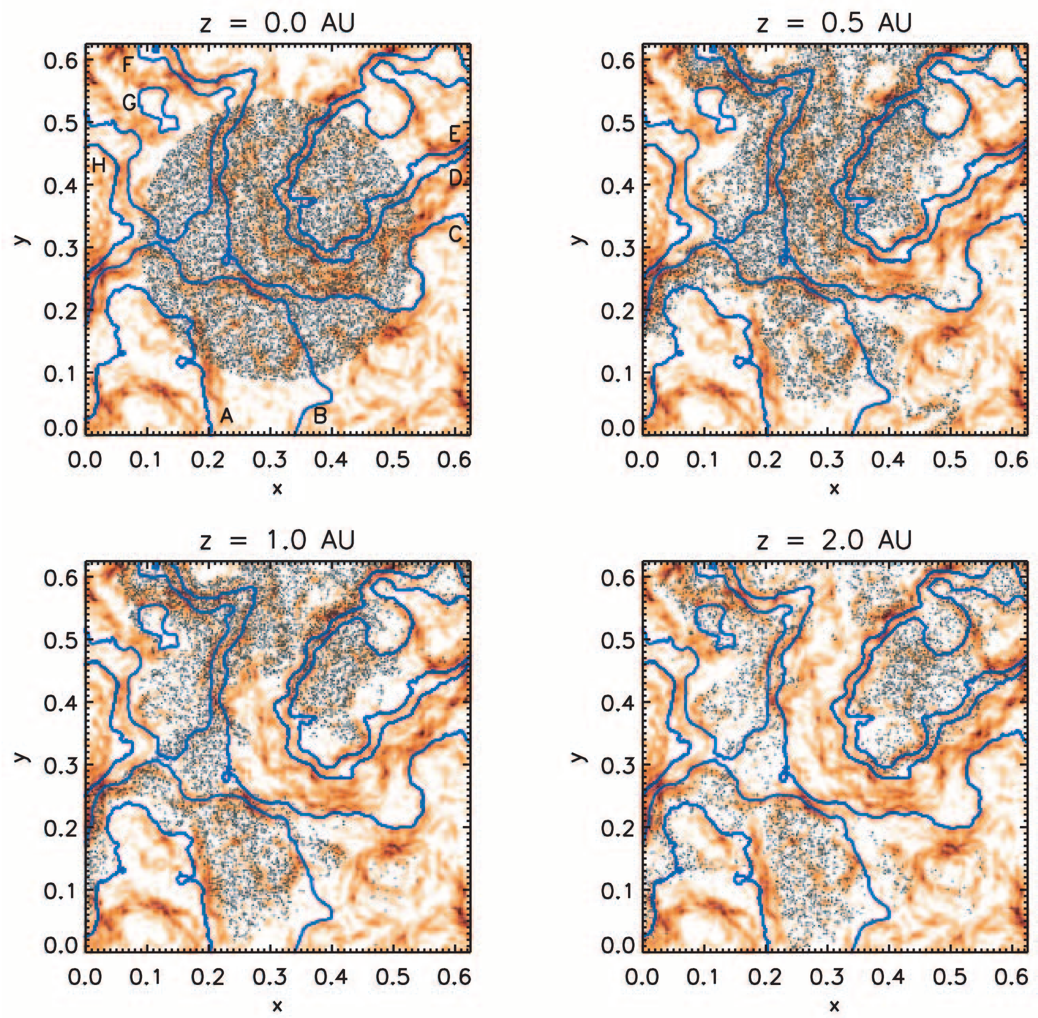

FIG. 12.—Scatter plots of magnetic field-line trajectories in 2D + slab turbulence at various distances z, for initial locations within a circular injection region at $z = 0$, for the same representation of 2D turbulence as in Fig. 11. The blue curves are the mathematically defined LTBs. The red shading indicates the value of $|b^{2D}|^2$ corresponding to the contour plot of $a(x, y)$ in Fig. 11.

In Figure 12, the best example of the success of LTBs at organizing trapping regions is provided by contours A and B (labeled in the top left panel). The region between these two equipotential contours effectively traps field lines over a distance $z > 2$ AU. In terms of O-points and X-points visually identified a priori in Figure 11, the strip between contours A and B includes three O-points and one X-point. However, these O-points apparently do not have individual trapping boundaries; the LTBs successfully delineate a merged trapping zone with sharp boundaries. Similarly, when viewing the contour plot of b_{2D}^2 in Figure 12 one would not a priori expect sharp gradients along the particular curves A and B. Thus, the sharp gradients are not identified by a strong 2D field alone, but rather by equipotential contours, that is, 2D orbits, across which the slab diffusion is apparently suppressed. The trapping zone between A and B is evidently not defined by a closed orbit around a single O-point or cluster of O-points; for example, it extends well beyond the three O-points identified in Figure 11. Contour A could be viewed as a trapping boundary enclosing a cluster of O-points, in which case it serves to delineate a zone that field lines are largely unable to cross into. In other words, LTBs define sharp boundaries of magnetic connectivity to the source, which can either trap or exclude the field lines of interest (e.g., those on which particles were injected by an impulsive solar flare).

The region between contours C and D is a similar strip with distinct magnetic connection. In this case, the 2D field is particularly strong within the strip, and a systematic motion of the field lines is evident as a function of z. The boundary of the injection region is convected through the strip, providing an example of a sharp gradient that is not associated with LTBs but rather with the boundary of injection at the source. Note, however, that gradients associated with the injection boundary move in (x, y) as a function of z and are less evident for $z > 1$ AU. The sharp gradients associated with LTBs are at fixed locations and are more persistent to large z.

Contours D and E in Figure 12 are local maxima of $\langle b_{2D}^2 \rangle$ that are rather close together. They can be viewed as surrounding a cluster of neighboring O-points, and they correspond to a major pocket of trapped field lines. Thus, these LTBs do conform to the expectation of Ruffolo et al. (2003) that field lines can be trapped in regions surrounding O-points. We see that the trapping region around O-points is indeed of limited extent (relevant to the "filling factor" issue raised by Kaghashvili et al. 2006) and the trapping boundary is defined by the "ridge" of high b_{2D}^2 surrounding this region.

TABLE 2

Comparison of Processes of Trapping and Diffusion of Magnetic Field Lines for a Uniform Mean Field plus Two-dimensional Field plus Slab Turbulence

Process	Gaussian 2D Island[a]	2D Turbulence[b]
Trapping	Within σ of the O-point	Within local trapping boundaries
Ensemble average diffusion	Slab diffusion	Combination of 2D and slab diffusion, 2D-dominated for solar wind conditions[c]
Motion within the trap	2D motion plus suppressed slab diffusion	2D motion plus slab diffusion
Escape from the trap	Suppressed slab diffusion	Suppressed slab diffusion
Requirements for suppression of diffusive escape	Strong 2D field	Moderate 2D field plus irregular 2D orbit

[a] The 2D field is defined by eqs. (12) and (13); see Fig. 1.
[b] See Fig. 2.
[c] Matthaeus et al. 1995.

Contour F again surrounds a cluster of O-points, with contour G nested inside at a higher level of $a(x, y)$. Contour G actually excludes field lines up to $z \approx 1$ AU; thereafter, those that did get in are effectively trapped and the region inside has a higher density than that outside. Contour F is reasonably successful at delineating sharp gradients along part of its length, in particular defining the outer edge of a region of trapped field lines at long z. However, the inner edge of that region is not well delineated by our LTBs. Note that for much of its length, F nearly coincides with C or with H. Yet, it does play a distinct role. There is an interesting triangular region between contours B, C, and F, which is not fully enclosed by LTBs yet does have a high density at $z = 1$ AU with a sharp gradient along C, followed by a low density at $z = 2$ AU with gradients along B and F. This type of behavior was not expected previously and seems to correspond to a plateau of unusually constant $a(x, y)$, that is, unusually low δb^{2D}. Field lines do flow into the triangle through the gap between B and C, but once there they flow more slowly, until finally evacuating systematically between $z = 1$ AU and $z = 2$ AU. Once again, the LTBs identify boundaries of distinct magnetic connectivity where strong gradients like these can occur, though in some cases such as contour H the LTB is simply not reached by field lines from the injection region over the z-range of interest.

Note that the LTBs are defined only with reference to the 2D field, with no knowledge of the injection region; in particular, they are not "tuned" to the size of the injection region. It is interesting that most of the LTBs in Figure 12 extend far beyond the injection region and are thus defined by an average over a contour extending far from the region of interest. A clear example is contour C, which extends very far and indeed appears to be an "open" contour over the scale of interest. Yet it somehow does effectively define a sharp gradient of field-line density at the edge of the triangle described above. A few persistent sharp gradients are not explained by the LTBs found by our procedure, including those noted earlier within contour F and a small group of trapped field lines to the right of contour B, corresponding to an O-point identified by eye in Figure 11. Nevertheless, the LTBs succeed in discriminating regions of distinct magnetic connectivity and in identifying almost all the sharp "dropout" gradients that are not directly associated with boundaries in the injection region.

One could say that the entire structure seen in Figure 12 is an interaction between the field-line random walk, which has regions of different connectivity as delineated by LTBs, and the boundary of the injection region at $z = 0$. If the injection region has a very wide lateral extent, that is, with no injection boundary over the region of interest, then there is simply a uniform density of field lines with no dropouts (Mazur et al. 2000; Giacalone et al. 2000). Observationally, this corresponds to the case of gradual solar events, for which dropouts are not found. In the context of 2D+slab turbulence, the uniform density follows from Liouville's theorem (Ruffolo et al. 2003).

Finally, we take into account the results of § 3, which indicate that a strong $\boldsymbol{b}^{2D}$ can directly contribute to field-line trapping by suppressing the diffusive escape. Now, in the case of a single Gaussian 2D island $\boldsymbol{b}^{2D}$ was strong throughout the core of the island, so a substantial difference for the turbulent 2D field is the concentration of b_{2D}^2 in narrow "ridges" as seen from the red shading in Figure 12. Thus, the suppression of diffusion in a turbulent 2D field, as demonstrated in § 4.1, is more concentrated along distinct trapping boundaries. The processes of field-line trapping and diffusion for the two types of 2D fields are summarized in Table 2. For the turbulent 2D field, the LTBs are apparently curves of low lateral diffusion, effectively separating regions of different magnetic connection to the source. The sharp gradients in the density of field lines connected to the injection region at the source are almost all associated with either (1) LTBs as defined by our mathematical prescription, with reference only to the 2D magnetic fluctuations, or (2) boundaries of the injection region.

5. SUMMARY AND CONCLUSIONS

Overall, the present study supports the basic idea that the dropout phenomenon, in which the observed SEP flux from impulsive solar flares rises and drops suddenly and nondispersively, is associated with filamentation of magnetic field line connection to the source (Mazur et al. 2000; Giacalone et al. 2000). The temporal features correspond to particle-rich magnetic filaments convecting past the spacecraft. The impulsive solar flare injects particles over a limited spatial region at the Sun (Reames 1992), and field lines connected to that region have a highly nonuniform distribution at 1 AU. In our view (Ruffolo et al. 2003), at 1 AU some field lines are still trapped in filamentary structures while others have escaped to travel far in the lateral directions. Here, using numerical experiments with model fields, we have shown that this is a natural consequence of anisotropic turbulence, which, for solar wind parameters, implies that the lateral motion of field lines cannot be viewed as uniformly diffusive over a scale of 1 AU.

In the 2D+slab model of magnetic turbulence, thought to be a relevant idealization of solar wind fluctuations, the average diffusion can be quite strong, as is indeed inferred from observations of the lateral transport of SEPs (Ruffolo et al. 2003; McKibben 2005). However, the contribution to the ensemble average diffusion coefficient due to the 2D fluctuations is dominant for these parameters, and the implied diffusive rate of lateral spread, while accurate for the ensemble as a whole, does not apply initially to field lines that start near an O-point of the 2D turbulence. Thus the small-scale topology of 2D turbulence plays a role in restricting the lateral motion of field lines, with some subset of field lines (those "trapped") approaching the full diffusive limit much more slowly than the ensemble average behavior. Furthermore, during the trapping phase the contribution of slab fluctuations to the field-line random walk is suppressed by a strong 2D field (Chuychai et al. 2005), an effect that further delays lateral spread. The present work shows that the ingredients of topological trapping and suppressed diffusive escape do apply to the 2D+slab model of turbulence with parameters suitable to describe the solar wind, and we can both qualitatively explain the sharp filamentation patterns and quantitatively explain their persistence beyond a distance of 1 AU. We note that the 2D+slab model is an idealized approximation, and we view the separate components as representing (1) the structure that causes trapping (2D part) and (2) the turbulence that induces escape (slab part). In reality the wavevector distribution should be broader, and for example, the 2D part might be generalized as a flux tube that varies weakly in the parallel direction (as in reduced MHD [Montgomery 1982; Zank & Matthaeus 1992] or the GS model [Goldreich & Sridhar 1995]). The slab component might generalize in a variety of ways to a broadband incoherent MHD wave spectrum.

To quantify the phenomena of trapping and diffusive escape of field lines from topological traps associated with transverse complexity of turbulence, we have introduced several concepts. For a specified 2D island, whether regularly shaped (Gaussian) or irregularly shaped (turbulence), we find that the advance of the mean squared lateral displacement toward its asymptotic untrapped limit is delayed by trapping, and the effect is enhanced when field lines start more deeply inside a 2D island. "Deeper" here means that the field line is insulated from the distant outside region by larger transverse (poloidal or 2D) magnetic flux. Quantifying this effect in a simple way leads to the notions of maximum trapping length, which occurs for the most deeply trapped field lines, and a critical radius (or value of the potential) beyond which field lines are too weakly trapped to see any delay in lateral transport at all. While some insight derives from this perspective, there are limitations: to quantify trapping in this way, one needs to look at one specific magnetic island, and furthermore, one needs to examine conditional statistics of many field lines.

To partially alleviate these difficulties, we introduced the notion of local trapping boundaries (LTBs). All closed 2D field lines might be viewed as potential trapping regions, but it turns out that islands with more flux contained in them, or more properly, more flux per unit radius, seem to provide better traps. This means that field lines with strong average 2D magnetic field strength (flux density) are good candidates to trap field lines effectively. These are the LTBs, which can be calculated from the 2D magnetic field alone, with no reference to the statistics of field lines. Nevertheless our numerical experiments show that the LTBs provide a good estimate of where trapping will occur.

We find from the above discussion that suppressed diffusion is an important process that is expected to contribute to the dropout features of field lines over a distance of 1 AU. The assumption is that the interplanetary magnetic field is highly structured in the direction transverse to the mean field, in the sense of 2D turbulence. Therefore, near injection regions field lines may be near either near O- or X-points, and for some span of distances, these lead to different rates of lateral spread. The field lines near the O-points experience suppressed diffusion and diffuse in the direction perpendicular to the mean field more slowly than the field lines near the X-points. Therefore, these different rates of spreading lead to inhomogeneous features and sharp gradients of the field-line density in the direction perpendicular to the mean field. If these field lines represent the guiding centers of the SEPs injected from a localized source near the Sun, the particles then follow those field lines. We find a dropout-like distribution of the field lines (surrogates for particles) at 1 AU if the size of the island is about 0.03 AU. From this study, we can say that the field lines can be trapped for distances longer or shorter than 1 AU, and also for trapping-island sizes that can be larger or smaller than 0.03 AU, depending on the magnetic field parameters as described above. Conversely, in principle our formulation of the trapping length might be used to analyze observed dropout features in conjunction with magnetic field parameters of the solar wind, using other methods to model or constrain the topology of the nearby magnetic field (Hu & Sonnerup 2003). In this way the present analysis may lead toward a physical explanation of the persistence, sharpness, and intermediate filling factor of dropouts of SEPs at Earth orbit, as found both in observations and in various independent simulation models.

The authors would like to thank Alejandro Sáiz and Nimit Kimpraphan for useful discussions. This study was supported by the Thailand Research Fund and the NASA Sun-Earth Connection Theory Program (grant NAG 5-8134).

REFERENCES

Bieber, J. W., Matthaeus, W. H., Shalchi, A., & Qin, G. 2004, Geophys. Res. Lett., 31, No. L10805
Bieber, J. W., Matthaeus, W. H., Smith, C. W., Wanner, W., Kallenrode, M.-B., & Wibberenz, G. 1994, ApJ, 420, 294
Bieber, J. W., Wanner, W., & Matthaeus, W. H. 1996, J. Geophys. Res., 101, 2511
Chuychai, P., Ruffolo, D., Matthaeus, W. H., & Rowlands, G. 2005, ApJ, 633, L49
Giacalone, J., Jokipii, J. R., & Matthaeus, W. H. 2006, ApJ, 641, L61
Giacalone, J., Jokipii, J. R., & Mazur, J. E. 2000, ApJ, 532, L75
Goldreich, P., & Sridhar, S. 1995, ApJ, 438, 763
Gosling, J. T., Skoug, R. M., McComas, D. J., & Mazur, J. E. 2004, ApJ, 614, 412
Gray, P. C., Pontius, D. H., Jr., & Matthaeus, W. H. 1996, Geophys. Res. Lett., 23, 965
Hu, Q., & Sonnerup, B. U. Ö. 2003, J. Geophys. Res., 108(A1), No. 1011
Jokipii, J. R. 1966, ApJ, 146, 480 (erratum 152, 671 [1968])
Jokipii, J. R., & Coleman, P. J., Jr. 1968, J. Geophys. Res., 73, 5495
Kaghashvili, E. Kh., Zank, G. P., & Webb, G. M. 2006, ApJ, 636, 1145
Leamon, R. J., Smith, C. W., & Ness, N. F. 1998, Geophys. Res. Lett., 25, 2505
Maron, J., Chandran, B. D., & Blackman, E. 2004, Phys. Rev. Lett., 92, No. 045001
Matthaeus, W. H., Goldstein, M. L., & Roberts, D. A. 1990, J. Geophys. Res., 95, 20673
Matthaeus, W. H., Gray, P. C., Pontius, D. H., Jr., & Bieber, J. W. 1995, Phys. Rev. Lett., 75, 2136
Matthaeus, W. H., Smith, C. W., & Bieber, J. W. 1999, in AIP Conf. Proc. 471, Solar Wind Nine, ed. S. R. Habbal et al. (Woodbury, NY: AIP), 511
Mazur, J. E., Mason, G. M., Dwyer, J. R., Giacalone, J., Jokipii, J. R., & Stone, E. C. 2000, ApJ, 532, L79
McKibben, R. B. 2005, Adv. Space Res., 35, 518
McKibben, R. B., Lopate, C., & Zhang, M. 2001, Space Sci. Rev., 97, 257
Montgomery, D. 1982, Phys. Scr., No. T2, 83
Narayan, R., & Medvedev, M. V. 2001, ApJ, 562, L129
Pommois, P., Zimbardo, G., & Veltri, P. 2005, Adv. Space Res., 35, 647
Press, W. H., Teukolsky, S. A., Vetterling, W. T., & Flannery, B. P. 1992, Numerical Recipes in FORTRAN (2nd ed.; Cambridge: Cambridge Univ. Press)
Reames, D. V. 1992, in IAU Colloq. 133, Eruptive Solar Flares, ed. Z. Švestka, B. V. Jackson, & M. E. Machado (Lecture Notes in Physics, 399) (Berlin: Springer), 180

Ruffolo, D., Matthaeus, W. H., & Chuychai, P. 2003, ApJ, 597, L169
Smith, C. W., Mullan, D. J., & Ness, N. F. 2004, J. Geophys. Res., 109, No. A01111
Smith, C. W., Mullan, D. J., Ness, N. F., Skoug, R. M., & Steinberg, J. 2001, J. Geophys. Res., 106, 18625
Zank, G. P., & Matthaeus, W. H. 1992, J. Plasma Phys., 48, 85
Zank, G. P., Matthaeus, W. H., Bieber, J. W., & Moraal, H. 1998, J. Geophys. Res., 103, 2085
Zank, G. P., Matthaeus, W. H., & Smith, C. W. 1996, J. Geophys. Res., 101, 17093
Zimbardo, G., Pommois, P., & Veltri, P. 2004, J. Geophys. Res., 109, No. A02113